J. Synchrotron Rad. (1998). **5**, 1270–1274

Angular Resolution of Parallel Foils on a Synchrotron Powder Diffractometer

M. A. Roberts[a] and C. C. Tang[b]*

[a]*Department of Physics and Astronomy, University College London, Gower Street, London WC1E 6BT, UK, and* [b]*CLRC Daresbury Laboratory, Warrington WA4 4AD, UK.*
E-mail: c.c.tang@dl.ac.uk

(*Received 10 February 1998; accepted 3 June 1998*)

In an attempt to improve the resolution in flat-plate diffraction geometry, a new set of parallel foils, 100 μm spacing, 365 mm long with an aperture of 20 × 20 mm^2, has been commissioned. The study was carried out using the two-circle diffractometer of station 2.3 at the SRS. In order to properly quantify the improvements, a detailed and comparative study of the instrumental resolution using the new and existing foils, of 200 μm spacing, is reported. A number of cubic materials, BaF_2, Si and CeO_2, that are known to show well defined Bragg peaks over the full 2θ angular range available, were investigated.

Keywords: synchrotron X-rays; high-resolution powder diffraction; parallel-foil collimators.

1. Introduction

Synchrotron-radiation-based diffractometry has become a very powerful technique for structural studies of polycrystalline materials due to the high flux, wavelength tunability and parallel-beam optics offered by the synchrotron radiation sources. Despite the development of new powder diffractometers on third-generation sources, *e.g.* BL16 at the European Synchrotron Radiation Facility (Fitch, 1996), further improvements are desirable. In the continued development of such instruments the demands from other diffraction techniques means that adaptability is also becoming an issue which must be considered for the longevity and efficiency of increasingly scarce resources.

The diffractometer on station 2.3 at the SRS (Daresbury) can perform diverse experimental measurements, with flat-plate powder, capillary diffraction (Cernik *et al.*, 1990; Collins *et al.*, 1992) and reflectivity studies (Tang *et al.*, 1998). For each type of experiment the diffraction geometry needs to be reconfigured. To this aim, a new 2θ-axis arm has been constructed, essentially comprising of an X-95 optical bench extending for approximately 70 cm, to which various components can be fixed to improve specific operations. Since the development of parallel foils (Parrish *et al.*, 1986; Hart & Parrish, 1986), they have been used to gain high intensity and good resolution on such instruments. The main role of the foils is to provide a high degree of diffraction collimation. A typical foils assembly is constructed from a set of stainless-steel foils of thickness 50 μm, 360 mm in length and spaced 200 μm apart. The gap and foil length define a nominal angular receiving aperture of ∼0.064°. In addition, there are other advantages of these parallel-foil receiving slits, such as the insensitivity to small changes in sample height (Hart & Parrish, 1986). The determination of instrumental characteristics, such as peak profile breadth and shape, are important precursors to the use of the instrument for the study of complex materials in a polycrystalline form by the Rietveld method (Rietveld, 1967, 1969), where severe overlap of reflections becomes inevitable.

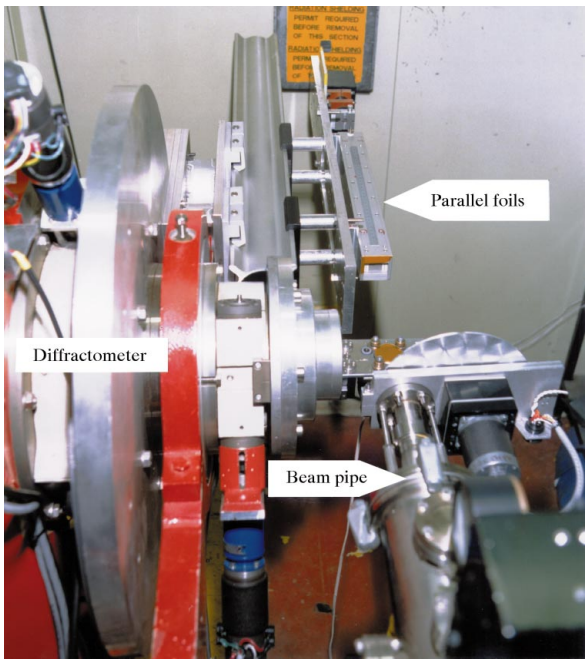

Figure 1
The PF1 slits mounted on the 2θ arm of the powder diffractometer on station 2.3 at Daresbury Laboratory. The photograph was taken with the camera looking at the apparatus from above the beam pipe. To reveal the parallel foils, the short vertical slits and the vacuum vessel were removed.

2. Instrumentation

The powder diffractometer on station 2.3 was initially constructed for ambient high-resolution powder-diffraction (HRPD) studies (Cernik *et al.*, 1990; Collins *et al.*, 1992). The centre of the instrument is situated approximately 15 m tangentially from a 1.2 T bending magnet in the 2 GeV electron storage ring. The beamline receives X-rays in the range 5–20 keV. The electron beam current is about 250 mA at the beginning of the fill and decays down to about 120 mA in 20 h. A recent detailed summary of the machine status for the synchrotron is given by Munro (1997). The polychromatic X-ray beam is monochromated by a channel-cut Si(111) single crystal which is thermally maintained at 303 ± 0.1 K. A 2 × 10 mm^2 monochromatic beam was used, defined by two pairs of centre-opening slits, and incident at the centre of the two-circle (θ and 2θ) diffractometer. A scintillation detector, mounted below the beamline, monitored the incident X-ray flux using a kapton foil set obliquely between the monochromator and the sample. The 'beam height' was surveyed and the axes of the diffractometer aligned using an optical leveller.

Fig. 1 shows a photograph of the instrument taken with the camera looking at the diffractometer from above the incident beam pipe. The flat-plate sample spinner is mounted on the θ-circle. The X-95 optical bench is bolted onto the 2θ-circle and the new design is shown in the photograph. This not only enables the change-over time between configurations to be greatly enhanced but is more 'user friendly'. The parallel-foils assembly can now be readily clamped onto the optical bench for HRPD data collection. The new parallel foils (PF1), of 100 μm spacing, manufactured by Rigaku, are similar to those used by Toraya *et al.* (1995), and are intended to be an improvement. However, the original foil assembly (PF2), of 200 μm spacing, giving a nominal resolution of 0.065°, is normally dedicated to the instrument for user application. Table 1 gives a selection of the foil assembly specifications, resulting in an enhanced nominal resolution of 0.031° for the PF1 slits. Additionally, a set of short vertical foils, of length 60 mm and spacing 1 mm (not shown in Fig. 1), are mounted in front of the parallel foils, resulting in an angular aperture of 1.9° and thus reducing the axial beam divergence. The parallel and vertical foils are housed in a vacuum vessel (not shown in Fig. 1) to reduce the background scattering level and the effects of air absorption.

3. Experimental and data analysis

A number of high-quality powder materials purchased from the National Bureau of Standards (USA), including BaF_2, CeO_2 and Si, were used to characterize and compare the performance of the two sets of parallel-foil assemblies. BaF_2 was used as the principal test material for the instrumental resolution since it is an ideal standard for these types of measurements due to the minimal strain within the polycrystallites, thus reducing any possible effects from sample strain broadening. The lattice parameter was refined to $a = 6.19871 \pm 0.0003$ Å, space group *Fm3m*. All reflections up to ~104° in 2θ were measured with $\lambda = 1.4000$ Å. Three different cycles of data collection were undertaken: the original 200 μm foils with the vertical scatter slits (the usual high-resolution configuration), and the new 100 μm foils with and without the axial-divergence

Table 1
Selected specifications for the PF1 and PF2 parallel-foil assemblies used on the HRPD instrument.

	PF1	PF2
Foil spacing (μm)	100	200
Foil length (mm)	365	355
Foil thickness (μm)	50	50
Effective window size (mm)	20 × 20	20 × 20
Foil flatness (μm)	~10	~10
Number of foils	~130	~80
Foil material	Stainless steel	Stainless steel
Angular aperture (°)	0.031	0.065

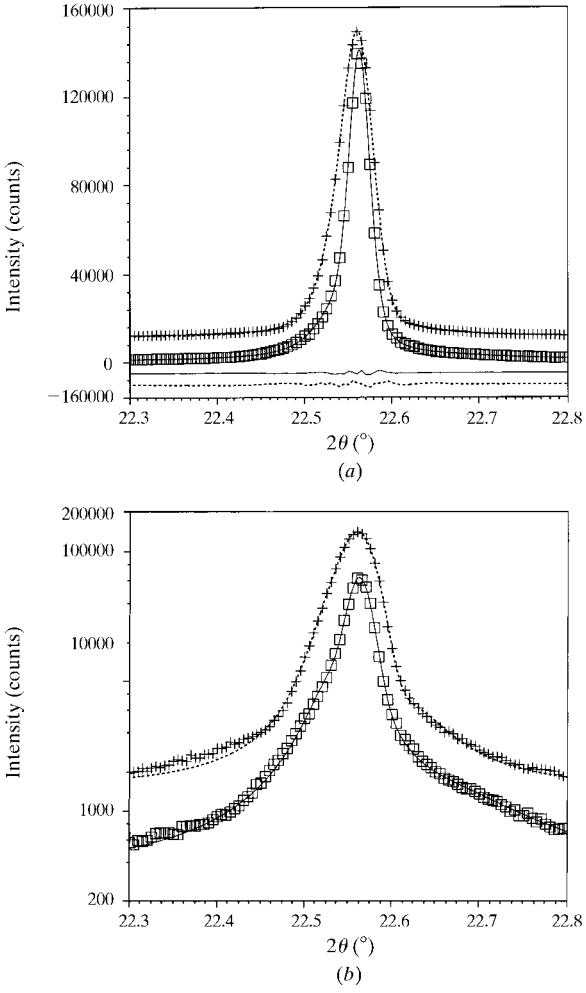

Figure 2
(*a*) The (111) reflection measured from BaF_2 using PF1 foils (squares) and PF2 foils (crosses). The corresponding fitted and difference profiles are shown by solid and dashed lines. For clarity the PF2 data have been shifted above the PF1 data. (*b*) The data are also plotted on a logarithmic scale to highlight the tail profiles.

scatter slits. In addition, scans of overlapping peaks from a mixture of CeO_2 and Si were obtained. These two standard materials were chosen due to their similar lattice parameters (*cf.* Si, $a = 5.43094$ Å, space group $Fd3m$, and CeO_2, $a = 5.4111$ Å, space group $Fm3m$) and, using an X-ray beam of $\lambda = 0.7500$ Å, the (111) Bragg reflections would overlap significantly. The mixture was prepared in a ratio of 25:75 such that the relative peak intensities would be similar. This would allow the performance of the PF1 and PF2 slits to be further compared.

The samples were mounted in flat-plate mode and scanned in $\theta/2\theta$ geometry. The profile intensity was scanned with a step size of 0.005° over a 2° angular range centred about the Bragg reflections. The materials, loaded into circular perspex holders used for reflection geometry, were rotated in the plane of the specimen surface during the data collection. Multiple scans of 1 or 2 s at each point were collected and summed together for improved statistics. The variation of the full width at half-maximum (FWHM) of Bragg reflections from BaF_2 was determined in the angular range 22–104° in 2θ. Individual Bragg reflections were analyzed using a composite peak profile comprised of a pseudo-Voigt and Gaussian functions. The program *PeakFit* (Jandel Scientific Software) performs least-squares refinements for parameters of a linear background level and peak parameters of maximum intensity amplitude, peak centre, FWHM and the mixing parameter. This profile conjugation proves to be an adequate description for the data collected using both the 100 µm and 200 µm foil assemblies (see §4). Intensity data were normalized using the incident beam monitor when necessary.

4. Results and discussion

Data for the (111) reflection ($2\theta = 22.56°$) of BaF_2, collected using the PF1 and PF2 slits, are illustrated in Fig. 2(*a*), and also plotted logarithmically to highlight the peak profile tails (Fig. 2*b*). To describe adequately the experimental profiles, it has been shown by Scardi *et al.* (1996) that the data can be modelled with a pseudo-Voigt function for the main peak and two Gaussian functions for the tails. The present data were treated in this fashion using the peak-fitting software, and the following equation describes the pseudo-Voigt form used,

$$y = a_0\left(\left\{\frac{a_3(\ln 2)^{1/2}}{a_2\pi^{1/2}}\exp\left[-4\ln 2\left(\frac{x-a_1}{a_2}\right)^2\right] + (1-a_3)\Big/\pi a_2\left[1+4\left(\frac{x-a_1}{a_2}\right)^2\right]\right\} \times\left[\frac{a_3(\ln 2)^{1/2}}{a_2\pi^{1/2}}+\frac{1-a_3}{\pi a_2}\right]^{-1}\right), \quad (1)$$

where a_0 is the amplitude, a_1 is the centre, a_2 is the FWHM (>0) and a_3 is the shape (≥0, ≤1), with 0 being pure Lorentzian and 1 being pure Gaussian.

The calculated results (lines) for both sets of observed data (points) shown in the figures are in excellent agreement, indicated by the difference curves (bottom lines). The narrower peak observed with PF1 suggests that an improvement in resolution has been achieved, the improvement being illustrated more dramatically in the logarithmic plots of Fig. 2(*b*). A FWHM of $0.02758 \pm 0.00005°$ was obtained for the PF1 profile, compared with $0.0424 \pm 0.0005°$ for the PF2 slits. However, the asymmetry is more pronounced for the narrower assembly and the peak-profile 'tails' are significantly broader, being more pronounced on the low-angle side, and this trend was also apparent on other diffractometers of this design (Toraya *et al.*, 1995).

Investigations into the cause of the asymmetry lead to the rotation of the PF1 slits through 180°, *i.e.* the foils were rotated 180° about an axis perpendicular to the plane of the measured scattering intensity. The peak profiles for the (111) reflection shown in Fig. 3 were taken with the foils before (squares) and after (crosses) the rotation, resulting in a peak shift to lower angle. This was caused by a change in the 2θ zero angle when the foils were re-mounted on the detector arm. Under normal powder measurements, the 2θ circle would have been calibrated using the first nine silicon reflections and then the peak positions could be measured reproducibly to within 1 mdeg. Clearly, the asymmetry can be related to imperfections in the foil assembly itself since the peak profile is similarly reversed. Possible contributions to the asymmetry could include specular reflectivity from the foil surfaces with the cumulative intensity being displaced from the Bragg position by non-parallelism of the foils. However, Toraya *et al.* (1995) did not find this reversal of asymmetry when rotating their foil assembly. Once this fact was apparent, the foils were always kept in one orientation such that comparisons between PF1 and PF2 could be systematically investigated.

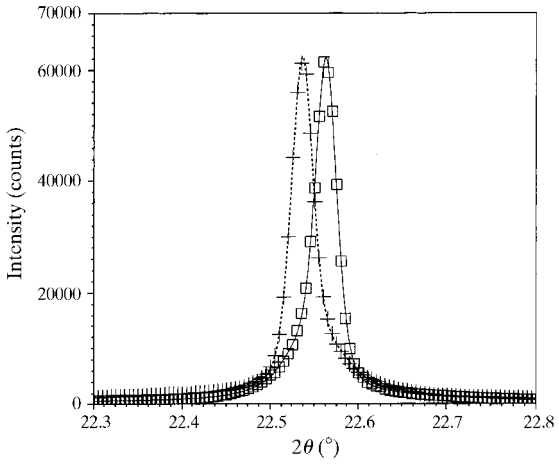

Figure 3
Scans of the (111) reflection using the PF1 slits at normal configuration (squares) and rotated through 180° (crosses). The corresponding fitted profiles are shown by solid and dashed lines, respectively.

The improvement in resolution is further illustrated in the profiles of Fig. 4, the observed and calculated profiles obtained by using the PF1 and PF2 foils for the overlapping Si(111) and CeO_2(111) reflections in the mixture. The data shown as crosses were taken using the PF2 foils. Clearly, the two peaks are better resolved when the PF1 foils were used (squares). Here, as observed before, the more pronounced tails may be a problem in integrated intensity extraction for structural analysis. However, with a proper representation of the profile using the appropriate peak functions described earlier, this problem can be overcome.

Fig. 5 shows the pseudo-Voigt FWHM as a function of 2θ angle measured from the BaF_2 sample. The new foils perform well without the scatter slits (triangles) at low angles but deteriorate more rapidly than the old foils (diamonds), the performance being marginally worse. On addition of the scatter slits the overall improvement in performance is quite marked (circles), with the FWHM approaching 0.028° at low diffraction angles. For each FWHM trend, a solid line defines the polynomial function. The standard errors for the data only become pronounced at high angles as the measurements were carried out on weaker Bragg peaks.

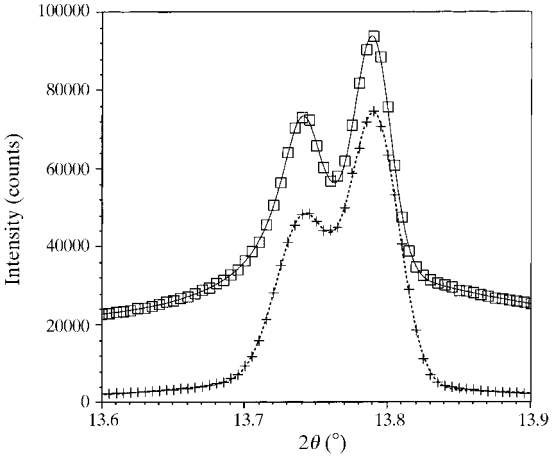

Figure 4
The observed (points) and calculated (lines) profiles for the (111) reflections of the CeO_2/Si mixture (λ = 0.7500 Å) using PF1 (squares) and PF2 (crosses). For clarity the PF1 data have been shifted above the PF2 data. Note that the PF1 peak profile is better resolved than that of PF2.

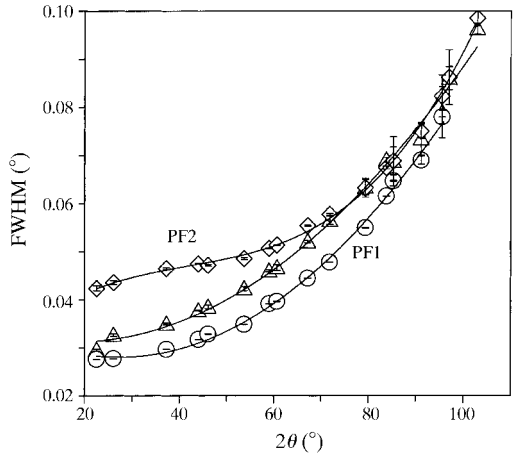

Figure 5
Variation of FWHM *versus* 2θ angle for BaF_2 measured using the PF1 slits with (circles) and without (triangles) axial divergence scatter slits, and the PF2 slits (diamonds). The corresponding polynomial fitted results are shown by solid lines.

Table 2
U, *V* and *W* peak-width parameters (see text) for the PF1 and PF2 foils in conjunction with the axial divergence scatter slits; values of the correlation coefficient *R* are also given.

	PF1	PF2
W	1.2910×10^{-3}	2.9182×10^{-3}
V	-3.7931×10^{-3}	-5.6024×10^{-3}
U	7.2699×10^{-3}	8.4522×10^{-3}
R	0.99771	0.99501

A general useful mathematical function to represent the instrument resolution of a powder diffractometer is the variation of the FWHM of the instrument line profiles with diffraction angle in quadratic form (Caglioti *et al.*, 1958; Langford *et al.*, 1991) as given below,

$$(\mathrm{FWHM})^2 = U\tan^2\theta + V\tan\theta + W, \qquad (2)$$

where the coefficients defining *U*, *V* and *W* from the definition of the peak width can be determined. The numerical coefficients for the PF1 and PF2 slits were obtained from the data shown in Fig. 5, and the results are summarized in Table 2. In both cases a good agreement of the quadratic law has been obtained as indicated by the high value of the correlation parameter *R*.

The average reduction in scattering intensity between the sets of foils was also determined. The intensity ratio of PF1, with and without the axial divergence scatter slits, to PF2 showed a considerable and almost constant reduction to 35% and 82%, respectively, as the foil spacing is reduced from 200 μm to 100 μm. This similarly signifies a reduction to 43% of the scattering intensity for PF1, purely by the addition of the vertical axial-divergence slits.

5. Conclusions

The addition of a new set of parallel foils (PF1) to the powder diffractometer on station 2.3 at the SRS (Daresbury) has improved the resolution function of the instrument, with a FWHM ranging from 0.02758 ± 0.00005° to 0.0779 ± 0.0014° over the angular range 22.56–95.55° in 2θ, determined using the standard material BaF_2. The lower value is approximately the nominal aperture of the parallel foils (*cf.* 0.031°). This is a distinct improvement of some 35% in resolution at low diffraction angles, over the original 200 μm foils (PF2). However, the existence of the broad peak tails of these foils must be considered in peak-profile fitting for structural refinement. The correct profile of the new foils consisted of a pseudo-Voigt function for the

main peak and two Gaussian functions for the tail features (see §4) and must be used to model the peak data throughout the entire powder pattern. It is likely that these tails are a consequence of slight curvature or non-parallelism or a reflectivity effect of the foils since the asymmetric nature of the peaks is reversible by rotating the foils through 180°. Nevertheless, the PF1 slits are ideal where high resolution for pattern indexing is required before complete structural characterization. Another inherent problem is the marked reduction in intensity, a notable characteristic when the diffraction is from weakly scattering materials. Thus, it is apparent that the actual configuration of the diffractometer is defined by the problem under investigation.

We would like to thank EPSRC for the provision of beam time. Our thanks also go to Alfie Neild for his technical assistance, and Matteo Leoni and Howard Millington for their help in the data analysis.

References

Caglioti, G., Paoletti, A. & Ricci, F. P. (1958). *Nucl. Instrum. Methods*, **3**, 223–228.
Cernik, R. J., Murray, P. K., Pattison, P. & Fitch, A. N. (1990). *J. Appl. Cryst.* **23**, 292–296.
Collins, S. P., Cernik, R. J., Pattison, P., Bell, A. T. M. & Fitch, A. N. (1992). *Rev. Sci. Instrum.* **63**, 1013–1014.
Fitch, A. N. (1996). *Mater. Sci. Forum*, **228/231**, 219–222.
Hart, M. & Parrish, W. (1986). *Mater. Sci. Forum*, **9**, 39–46.
Langford, J. I., Cernik, R. J. & Louër, D. (1991). *J. Appl Cryst.* **24**, 913–919.
Munro, I. H. (1997). *J. Synchrotron Rad.* **4**, 344–358.
Parrish, W., Hart, M., Erickson, C. G., Masciocchi, N. & Huang, T. C. (1986). *Adv. X-ray Anal.* **29**, 243–250.
Rietveld, H. M. (1967). *Acta Cryst.* **22**, 151–152.
Rietveld, H. M. (1969). *J. Appl. Cryst.* **2**, 65–71.
Scardi, P., Leoni, M., Cappuccio, G., Langford, J. I. & Cernik, R. J. (1996). *Mater. Sci. Forum*, **228/231**, 207–212.
Tang, C. C., Collins, S. P., Murphy, B. M., Telling, N. D., Wogelius, R. A. & Teat, S. J. (1998). *Rev. Sci. Instrum.* **69**, 1224–1229.
Toraya, H., Takata, M., Hibino, H., Yoshino, J. & Ohsumi, K. (1995). *J. Synchrotron Rad.* **2**, 143–147.